Applied Radiation and Isotopes 92 (2014) 58–72

Contents lists available at ScienceDirect

Applied Radiation and Isotopes

journal homepage: www.elsevier.com/locate/apradiso

A comparative evaluation of the CF:CS and CRS models in ^{210}Pb chronological studies applied to hydrographic basins in Brazil

D.M. Bonotto [a,*], R. García-Tenorio [b]

[a] Departamento de Petrologia e Metalogenia, Universidade Estadual Paulista (UNESP), Av. 24-A No. 1515, C.P. 178, CEP 13506-900, Rio Claro, São Paulo, Brazil
[b] Departamento de Física Aplicada II, Universidad de Sevilla, Av. Reina Mercedes No. 2, 41012 Sevilla, Spain

HIGHLIGHTS

- Comparative evaluation of the excess ^{210}Pb CF:CS and CRS models.
- Superior performance of the CRS model for evaluating sedimentation rates.
- Superior performance of the CRS model for chronological applications.
- Use of SiO_2–LOI concentration fluctuations for indicating heavy metal releases.

ARTICLE INFO

Article history:
Received 27 February 2014
Received in revised form
7 June 2014
Accepted 13 June 2014
Available online 25 June 2014

Keywords:
^{210}Pb-method
CF:CS model
CRS model
Sedimentation rate
SiO_2–LOI trends

ABSTRACT

The Constant Flux: Constant Sedimentation (CF:CS) and Constant Rate of Supply (CRS) of unsupported/excess ^{210}Pb models have been applied to a ^{210}Pb data set providing of eighteen sediments profiles sampled at four riverine systems occurring in Brazil, South America: Corumbataí River basin (S1=Site 1, São Paulo State), Atibaia River basin (S2=Site 2, São Paulo State), Ribeirão dos Bagres basin (S3=Site 3, São Paulo State) and Amazon River mouth (S4=Site 4, Amapá State). These sites were chosen for a comparative evaluation of the performance of the CF:CS and CRS models due to their pronounced differences on the geographical location, geological context, soil composition, biodiversity, climate, rainfall, and water flow regime, among other variable aspects. However, all sediments cores exhibited a common denominator consisting on a database built from the use of the same techniques for acquiring the sediments major chemical composition (SiO_2, Al_2O_3, Na_2O, K_2O, CaO, MgO, Fe_2O_3, MnO, P_2O_5, TiO_2 and LOI-Loss on Ignition) and unsupported/excess ^{210}Pb activity data. In terms of sedimentation rates, the performance of the CRS model was better than that of the CF:CS model as it yielded values more compatible with those expected from field evidences. Under the chronological point of view, the CRS model always provided ages within the permitted range of the ^{210}Pb-method in the studied sites, whereas the CF:CS model predicted some values above 150 years. The SiO_2 content decreased in accordance with the LOI increase in all cores analyzed and such inverse relationship was also tracked in the SiO_2–LOI curves of historical trends. The SiO_2–LOI concentration fluctuations in sites S1 and S3 also coincided with some Cu and Cr inputs in the drainage systems.

1. Introduction

^{210}Pb is an intermediary member of the natural ^{238}U decay series that finishes at the stable ^{206}Pb. The ^{238}U descendants are produced continuously in rocks and minerals, since uranium is among the main elements contributing to natural terrestrial radioactivity. ^{210}Pb is generated after the production of the gas ^{222}Rn in the ^{238}U decay series. Because a fraction of this gas escapes from the rocks, minerals and soils to the surrounding fluid phase, such as air, ^{222}Rn emanating from land surfaces is responsible for ^{210}Pb present in the atmosphere.

The fallout ^{210}Pb has been generally assumed to have a constant flux at a given site when averaged over a period of one year or more but its amount may vary from place to place depending on factors such as rainfall and geographical location. The atmospheric ^{210}Pb returning to the earth's surface has been commonly referred to as unsupported (excess) ^{210}Pb, $^{210}Pb_{xs}$, whereas the ^{210}Pb resulting from the decay of ^{238}U within rocks, soils, minerals and sediments has been termed supported (in situ produced) ^{210}Pb, $^{210}Pb_s$ (Eakins and Morrison, 1978).

* Corresponding author.
E-mail address: danielbonotto@yahoo.com.br (D.M. Bonotto).

http://dx.doi.org/10.1016/j.apradiso.2014.06.012
0969-8043/

The ^{210}Pb method of age dating was first outlined by Goldberg (1963) in a study to determine the rate of snow accumulation in Greenland and since the adaptation of the basic methodology by Krishnaswami et al. (1971) to the dating of lake sediments, numerous contributions have appeared in the field of ^{210}Pb geochronology. Thus, ^{210}Pb is today the most important geochronometer for sedimentary geologists/geochemists working with samples deposited in the past 100–150 years. For example, ^{210}Pb data have been used in sediments accumulation and mixing studies in lakes, estuarine, marsh, coastal areas and riverine systems that have been applied to limnology, including the evaluation of accelerated eutrophication, recent history of heavy metal pollution, influx rates for contaminants, regional erosion rates, salt marsh accretion and sediment budgets (see, e.g. Benninger et al., 1975; Evans and Rigler, 1980; Abril et al., 1992; Baskaran et al., 1996; Santschi et al., 2001; San Miguel et al., 2001, 2003, 2004; Martín et al., 2002; Jweda and Baskaran, 2011).

Several models for ^{210}Pb analysis have been developed using the radioactive decay equation, which were developed and refined to accommodate different environmental and anthropogenic influences as well as geological and sediment processes (see, for instance, Appleby and Oldfield, 1992; Abril, 2003, 2004). As with all models, there are certain assumptions that are accepted, and specific models may have additional assumptions and constraints. In general, the major assumptions are (Pennington et al., 1976; Noller, 2000): ^{210}Pb is quickly removed from the atmosphere and freshwater streams and sequestered in soils and sediments; ^{210}Pb is immobile once deposited; unsupported ^{210}Pb does not migrate down into the sedimentary column; supported ^{210}Pb is in secular equilibrium with its ancestor ^{226}Ra; unsupported ^{210}Pb is independent of depth.

The Constant Flux: Constant Sedimentation (CF:CS) and Constant Rate of Supply (CRS) models have been used to calculate sediment age at sample depth. The main distinction between them is that CRS assumes a constant atmospheric flux of ^{210}Pb and variable influx rate of sediments, whereas CF:CS is governed by a constant sedimentation accumulation rate. The vast literature on the use of the ^{210}Pb chronological methods indicates that the CRS model is the most widely used.

In Brazil, the ^{210}Pb-derived chronology was mainly developed in environments of slow deposition like lakes and of intense energetic activity like estuaries due to its long coastal area (Godoy et al., 1998a, 1998b). However, the sediments of rivers also contain a repository of valuable historical information on the temporal changes of population growth and industrial development. There is a significant less number of studies providing reliable radiochemical dates in Brazilian riverine sediments, due to difficulties on obtaining ^{210}Pb concentration data that are above the detection limit of the technique utilized and that are not affected by sediment mixing. Among the exceptions are the studies held by Bonotto and Lima (2006), Sabaris and Bonotto (2011), Nery and Bonotto (2011) and Matamet and Bonotto (2013) who applied the CF:CS model to four different riverine environments. On other hand, some gaps/doubts were found, with possible implications on the calculated ages and respective historical events of heavy metal inputs. Thus, the purpose of this paper is to compare the performance of the CF:CS and CRS models in four hydrographic basins previously studied in Brazil with the aim of verifying their applicability for the age generation over the last 100–150 years.

2. Theoretical review

The CF:CS (Constant Flux: Constant Sedimentation) model assumes that the incorporation of unsupported/excess ^{210}Pb to the sediments is produced at a constant flux and that the sedimentation rate is also constant (San Miguel et al., 2001). This implies that the concentration of unsupported ^{210}Pb in the initial sediments bed is constant. Additionally, the radioactive disequilibrium in the U decay series generally caused by ^{222}Rn loss from sediments has to be considered, since it would cause a depletion of supported ^{210}Pb, leading to non-equilibrium conditions between ^{226}Ra and ^{210}Pb (Imboden and Stiller, 1982; Ravichandran et al., 1995). Thus, the sedimentation rate is constant in the CF:CS model during the investigated period of time, producing an exponential diminution of the ^{210}Pb activity in accordance with the depth of the sediments column

$$^{210}\mathrm{Pb}_{xs(z)} = {}^{210}\mathrm{Pb}_{xs(0)} e^{-\lambda_{210} t} \quad (1)$$

where $^{210}\mathrm{Pb}_{xs(0)}$ represents the unsupported/excess ^{210}Pb activity at the sediment–water interface (or bottom of the uniformly mixed layer), $^{210}\mathrm{Pb}_{xs(z)}$ is the excess ^{210}Pb activity at z depth, λ_{210} is the radioactive decay constant for ^{210}Pb (0.0311 yr^{-1}), and t is the deposition time (age, in years).

The cumulative dry surface mass, CDSM (g cm^{-2}), is related to the deposition time according to the expression $t = \mathrm{CDSM}/f$, where f is the sediment mass flux (sedimentation rate, g cm^{-2} yr^{-1}). Eq. (1) can be simplified and rewritten as

$$\ln {}^{210}\mathrm{Pb}_{xs(z)} - \ln {}^{210}\mathrm{Pb}_{xs(0)} = (-\lambda_{210}/f) \times \mathrm{CDSM} \quad (2)$$

Plotting ln $^{210}\mathrm{Pb}_{xs(z)}$ against CDSM yields a straight line with slope $-\lambda_{210}/f$. The sedimentation rate f may then be determined using the least-squares fit procedure (Baskaran and Naidu, 1995).

In view of the pronounced environmental changes that have occurred over the past 150 years, rates of erosion and sediment accumulation may be expected to have varied significantly during this period. Where this has occurred, unsupported ^{210}Pb activity will vary with depth in a more complicated way and ^{210}Pb profiles (plotted logarithmically) will be non-linear. The methodology for calculating dates developed by Appleby and Oldfield (1978) and Robbins (1978) but within the assumptions set out by Krishnaswami et al. (1971) has become known as the Constant Rate of ^{210}Pb Supply (CRS) model. The ^{210}Pb age calculations are based here on the assumption that for a certain aquatic system the total annual unsupported ^{210}Pb fluxes delivered to, and maintained by, a depositional sequence should be constant during the past two centuries. The age of a certain level in a given depositional sequence would depend on the remained ^{210}Pb activity beneath this level relative to the integrated ^{210}Pb activity of the sequence (El-Daoushy, 1988). Although the total annual flux of ^{210}Pb could be considered constant, internal processes may influence the distribution and depositions of the available ^{210}Pb both vertically and horizontally. Assuming that internal and external processes controlling the mass-balance of a specific aquatic system have been stable during the past two centuries or so the ^{210}Pb flux at an arbitrary surface area could be given as (El-Daoushy, 1988):

$$F_{210} = \lambda_{210}.A_0 = \lambda_{210}.\sum_{m=0}^{m=\infty} C(m)dm \quad (3)$$

where F_{210} is the annual unsupported ^{210}Pb flux at a certain site, A_0 is the cumulative inventory of unsupported ^{210}Pb of the depositional sequence from mass zero at the surface to mass ∞ at which only supported ^{210}Pb exists and $C(m)$ is the ^{210}Pb concentration in a layer of mass dm. The age t of a certain level at which the cumulative specific activity of unsupported ^{210}Pb integrated over the whole profile (A_0, total inventory) has declined to A_x (the cumulative activity integrated for the part of profile below the depth x) satisfies the equation (Kotarba et al., 2002)

$$A_x = A_0 e^{-\lambda_{210} t} \text{ or } t = (1/\lambda_{210}) \ln(A_0/A_x) \quad (4)$$

The ages of the sediment layers can be used to calculate apparent sedimentation rates for each layer. This was done here

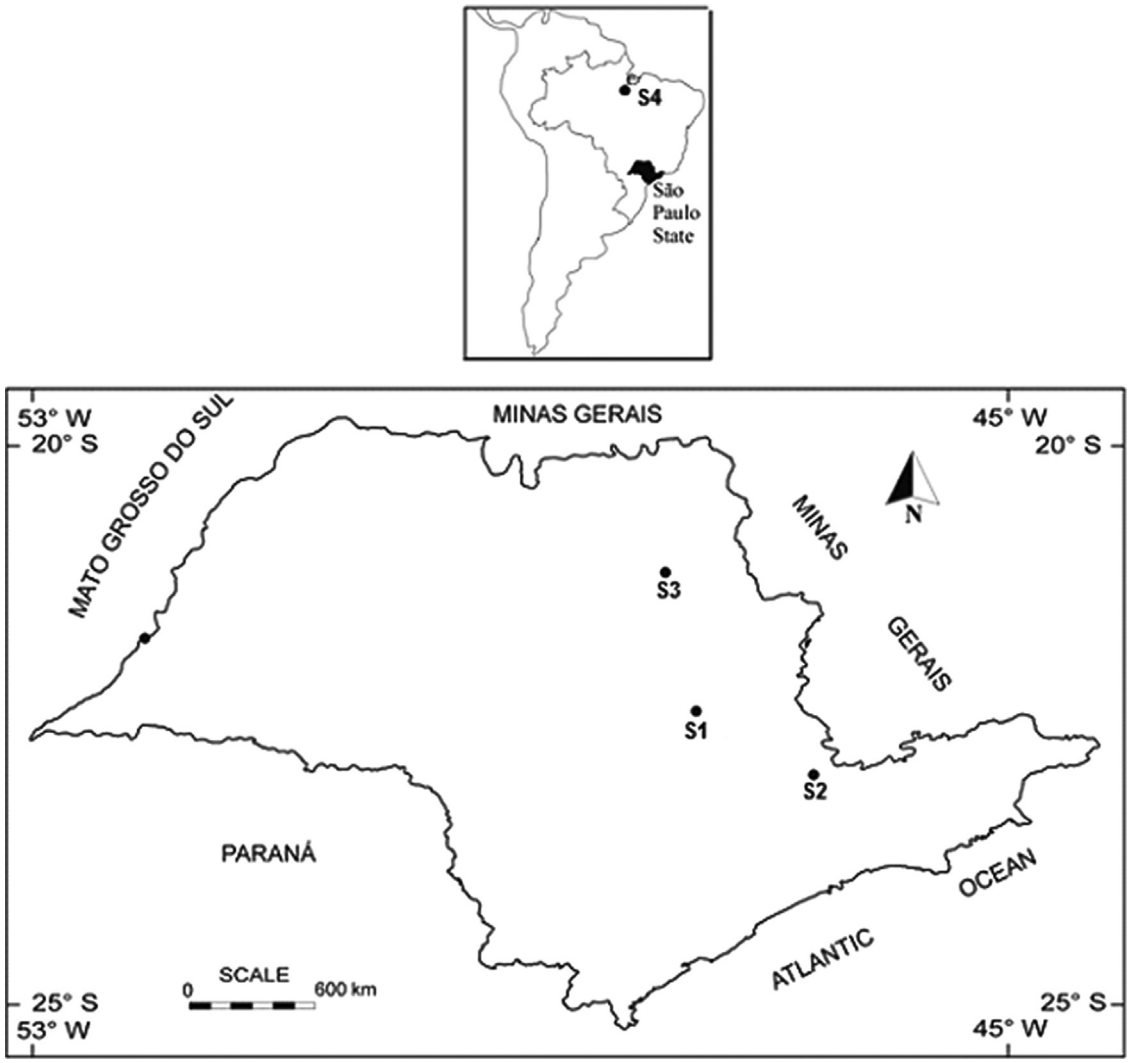

Fig. 1. A simplified map of the location of the sites in Brazil considered in this paper: Corumbataí River basin (S1=Site 1, São Paulo State), Atibaia River basin (S2=Site 2, São Paulo State), Ribeirão dos Bagres basin (S3=Site 3, São Paulo State) and Amazon River mouth (S4=Site 4, Amapá State). More details of each site are given by Bonotto and Lima (2006), Sabaris and Bonotto (2011), Nery and Bonotto (2011) and Matamet and Bonotto (2013).

considering that the age represents the center of the layer and adopting the following equation modified from Kotarba et al. (2002):

$$r_n = (w_n - w_{n-1})/(t_n - t_{n-1}) \quad (5)$$

where r_n is the sedimentation rate for the interval between centers of the $n-1$ and n-th layer, w_n and t_n are cumulative dry surface mass and age of the n-th layer, w_{n-1} and t_{n-1} are cumulative dry surface mass and age of the $n-1$ layer, $w_0=0$, $t_0=0$.

3. Methods and database

The selected sites for this study are located in São Paulo and Amapá states in Brazil and comprise (Fig. 1): Corumbataí River basin (S1=Site 1), Atibaia River basin (S2=Site 2), Ribeirão dos Bagres basin (S3=Site 3) and Amazon River mouth (S4=Site 4). They have been subjected to previous studies utilizing the ^{210}Pb-method (CF:CS model) as detailed by Bonotto and Lima (2006), Sabaris and Bonotto (2011), Nery and Bonotto (2011) and Matamet and Bonotto (2013). The sampling campaigns were held in different periods, i.e. years 1998 (S1), 2005 (S2), 2006 (S4) and 2010 (S3). They have been chosen due to the pronounced differences on the geographical location, geological context, soil composition, biodiversity, climate, rainfall, water flow regime and others variable aspects. On other hand, there is a common denominator coupled to the 18 sediments profiles analyzed, consisting on a database built from the use of the same techniques for acquiring the chemical composition and unsupported/excess ^{210}Pb activity data.

The cores were taken with a Wildco Model 77263 hand core sediment sampler in sites S1, S2 and S3. It consists of a stainless steel liner type core tube including screw-on Lexan nose piece, a plastic eggshell type core catcher to hold sample intact during extraction, and a transparent acrylic 51 cm long (5 cm internal diameter) liner tube that received the sample. In site S4, a 1–1.1 m long PVC tube (7.5 cm in diameter) was driven into the sediments. The cores were stored refrigerated (~2 °C) until sectioned, extruded in the lab and cut into 2–6 cm sections (sites S1, S2 and S3) or 10 cm thick slices (site S4). Each core was dried, pulverized, separated in different aliquots and stored in plastic bags for use in grain size evaluation and chemical/radionuclides analysis.

The major oxides in all slices were determined in one ~5 g aliquot by the X-ray fluorescence method. The chemical balance (in percentage) also supplied data on the loss on ignition (LOI), as the measurements involved weight loss of the samples after their

burning at selected temperatures. All SiO_2 and LOI contents are given in Table 1 for further discussion in the next section.

The total ^{210}Pb activity in the sediments, $^{210}Pb_T$, was determined by quantification of its granddaughter ^{210}Po (Karali et al., 1996). A known amount of ^{209}Po spike was added at the beginning of the digestion process to assess ^{210}Po recovery. Polonium was plated onto a copper disc (1-in. diameter) suspended in the solution placed on a hot plate magnetic stirrer, which was heated to ~80 °C and stirred during 75–90 min with a Teflon stirrer (Flynn, 1968). Then, the disc was removed, washed with demineralized water, dried in a heating lamp, and counted by conventional alpha spectroscopy with Si(Au) surface barrier detectors. The detectors were coupled to EG&G Ortec multichannel buffer and the MAESTRO software allowed plotting the α-spectrum containing the ^{209}Po and ^{210}Po peaks. In general, the analytical precision was between 10% and 20%, reflecting the use of an uncertainty of $\pm 1\sigma$ standard deviation for the counting statistics, the error propagation theoretical approach, and the low counting rate in some peaks in the α-spectra.

To obtain information about the parent-supported (in situ produced) ^{210}Pb, $^{210}Pb_s$, two techniques were adopted, depending on the available amount of material. For larger quantities (15–100 g), measurements of equivalent uranium, eU ($^{214}Bi = ^{226}Ra$), were performed by γ-ray spectrometry through a 2" × 2" NaI(Tl) scintillation detector and a 2048-channels multichannel analyzer provided by Ortec Ace 2K hardware controlled by MAESTRO software. For smaller portions of material (~1 g), measurements of ^{238}U content were done by α-spectrometry after several radiochemical steps that started with addition of a known amount of ^{232}U–^{228}Th spike at the beginning of each digestion process (Bonotto, 2010). ^{238}U was electrodeposited on stainless-steel planchets for assay by α-spectrometry using the same Si(Au) detectors utilized for ^{210}Po measurements. The critical level L_c (Currie, 1968) for acceptance of a positive measurement in the ^{238}U energy region was 0.000827 cpm.

The ^{222}Rn-loss from sediments was corrected adopting the findings of Bonotto and Caprioglio (2002) who realized laboratory time-scale experiments with different samples of sedimentary rocks in order to evaluate the radon release. An average value of the emanation coefficient E corresponding to 0.84 was found, indicating that only 16% of the ^{222}Rn generated by ^{226}Ra decay contributes to the production of ^{210}Pb. Such factor was utilized in all sediments analyzed for providing the $^{210}Pb_s$ data.

The excess ^{210}Pb activity, $^{210}Pb_{xs}$, was calculated as the difference between total and supported activities, i.e. $^{210}Pb_{xs} = ^{210}Pb_T - ^{210}Pb_s$. All $^{210}Pb_{xs}$ data for following discussion are shown in Table 1, including the depth interval of the sections in each sediments profile and the correspondent CDSM.

4. Results and discussion

4.1. Sedimentation rates by the CF:CS and CRS models

Table 1 reports the $\ln(^{210}Pb_{xs})$ data calculated from the ^{210}Pb excess activity in the core sediments profiles considered in this paper. The sediment mass fluxes by the CF:CS model were obtained by plotting the linear regressions of $\ln(^{210}Pb_{xs})$ activities against the CDSM for all individual cores (Figs. 2 and 3). The CDSM was plotted instead of core depth in order to eliminate possible errors that may arise due to sediment compaction (Robbins, 1978; Baskaran and Naidu, 1995). In some cases, the data of the more superficial and deeper layers of the profiles were disregarded for avoiding non validity of the steady-state accumulation as well assumed by Eakins and Morrison (1978), Baskaran and Naidu (1995), Turner and Delorme (1996) and Santschi et al. (2001), among others. The significance level (one-tailed probability value; 2 degrees of freedom) of the Pearson correlation coefficient obtained for the least-squares best fit was acceptable at 0.05 in most situations, however, in some cases, it was 0.10 (7) or 0.20 (3). The slopes of the best fits and sedimentation rates are given in Table 2, ranging, respectively, from −0.652 (3°) to −0.012 (68°) and from 0.05 to 2.51 g cm^{-2} yr^{-1}. Two different sedimentation rates were found by the CF:CS model in each sediments profile sampled at the Amazon River mouth (S4), whose mean values are: 0.91 g cm^{-2} yr^{-1} (AMZ1), 1.21 g cm^{-2} yr^{-1} (AMZ2) and 2.12 g cm^{-2} yr^{-1} (AMZ3). The same occurred in monitoring point RX3 at Ribeirão dos Bagres basin (S3) where the mean value is 0.32 g cm^{-2} yr^{-1}. Higher slopes of the straight lines implied on greater sedimentation rates, as expected and shown in Fig. 4a. Both parameters obeyed the exponential equation $f = 3.7909\exp^{(\text{slope}/0.0218)} + 0.1893$ ($r^2 = 0.98$) as fitted by Origin 7.5 software.

According to the premises of the CRS model, variable sedimentation rates occur along the sediments profile and all values obtained on using Eq. (5) are given in Table 1. They ranged from 0 at the core surface to 12.2 g cm^{-2} yr^{-1} in the 35-cm deep layer of the sampling point AMZ1 at S4. There is no systematic variation of the sedimentation rates according to the sediments core depth (or CDSM) as they sometimes may increase or decrease. However, there is a significant relationship between the sedimentation rates obtained by the CF:CS model (Table 2) and the mean values of the sedimentation rates estimated by the CRS model (Table 1) as shown in Fig. 4b. Thus, the highest rates were predicted by both models in the Amazon River mouth (S4), as expected, and, consequently, they appear to respond congruently to the different sedimentation rates occurring in the sites.

On other hand, the sedimentation rate of 0.73 g cm^{-2} yr^{-1} obtained by the CF:CS model in the sediments core AMZ1 sampled at site S4 (Table 2) is lower than other values calculated by the CF:CS model in much smaller basins, for instance: 0.80 g cm^{-2} yr^{-1} (S1 – Ajapi), 0.78 g cm^{-2} yr^{-1} (S3–RX1; S2 – point 1) and 0.76 g cm^{-2} yr^{-1} (S2 – points 4 and 9) (Table 2). The same has been verified with the sedimentation rate of 0.44 g cm^{-2} yr^{-1} in the sediments core AMZ2 sampled at the same site (Table 2) that is inclusively lower than 0.56 g cm^{-2} yr^{-1} (S3 – RX3), 0.49 g cm^{-2} yr^{-1} (S2 – point 6) and 0.53 g cm^{-2} yr^{-1} (S2 – point 7) (Table 2). Thus, such rates estimated by the CF:CS model in the Amazon River mouth do not agree with the expected huge sediments loads occurring there as higher values should be found, at least equivalent to 1.10 g cm^{-2} yr^{-1} (S4 – point AMZ1) or 1.97 g cm^{-2} yr^{-1} (S4 – point AMZ2) (Table 2).

Interestingly, all mean values of the sedimentation rates estimated by the CRS model in the sediments cores AMZ1, AMZ2 and AMZ3 sampled at site S4 (Table 1) were always higher than those found in other basins, agreeing with the huge expected sediments inputs in the area. In terms of other basins (S1, S2 and S3), the highest mean value was 1.02 g cm^{-2} yr^{-1} (S3 – RX6) (Table 1) that is 2.5–2.8 times lower than the mean sedimentation rates calculated by the CRS model in the monitoring points AMZ1, AMZ2 and AMZ3 (S4, Table 1). Therefore, there is a sharp contrast of the rates estimated by the CF:CS and CRS models in the Amazon area when they are compared to the values obtained for the smaller basins studied here. The performance of the CRS model on this aspect is better than that of the CF:CS model as it yields sedimentation rates values more compatible with those expected from field evidences.

4.2. Chronological perspectives by the CF:CS and CRS models

The deposition times estimated by the CF:CS and CRS models are given in Table 1. There is a significant relationship among the deposition times obtained by both models (Pearson correlation coefficient $r = 0.58$) as shown in Fig. 4c. Thus, in general, they

Table 1
Analytical data summary of the sediments cores considered in this paper. The locations of sites S1, S2, S3 and S4 are given in Fig. 1.

Depth range (cm)	Mean depth (cm)	Cumulative dry surface mass, CDSM (g cm^{-2})	SiO_2 (%)	LOI (%)	Excess ^{210}Pb activity, $^{210}Pb_{xs}$ (dpm/g)	ln ($^{210}Pb_{xs}$) (dpm/g)	Deposition time[a] (years) CF:CS model	Deposition year CF:CS model	Deposition time[b] (years) CRS model	Deposition year CRS model	Sedimentation rate[c] (g cm^{-2} yr^{-1}) CRS model
Ajapi (S1=Site 1)[d]											
0–2.5	1.2	3.76	82.80	3.18	0.47	−0.76	5	1993	0	1998	0
2.5–4.5	3.5	7.52	84.53	3.08	0.71	−0.34	9	1989	4	1994	0.91
4.5–6.5	5.5	10.87	82.78	3.76	0.72	−0.33	14	1984	12	1986	0.45
6.5–8.5	7.5	14.68	80.34	4.70	0.49	−0.71	18	1980	21	1977	0.39
8.5–10.5	9.5	18.74	85.91	3.17	0.56	−0.58	23	1975	30	1968	0.45
10.5–12.5	11.5	23.17	82.67	2.32	0.38	−0.97	29	1969	45	1953	0.30
12.5–18.5	15.5	31.79	88.05	2.37	0.58	−0.54	40	1958	61	1937	0.53
										Mean	0.50
Piracicaba (S1=Site 1)[d]											
0–2.5	1.2	1.71	63.59	9.22	1.88	0.63	8	1990	0	1998	0
2.5–4.5	3.5	2.59	62.65	10.29	2.28	0.82	12	1986	6	1992	0.15
4.5–7.0	5.7	3.86	69.73	8.15	2.04	0.71	18	1980	14	1984	0.15
7.0–9.0	8.0	5.00	65.76	9.64	1.99	0.69	23	1975	24	1974	0.12
9.0–11.5	10.2	6.81	79.32	5.51	1.36	0.31	31	1967	37	1961	0.13
11.5–14.0	12.7	9.02	84.21	3.91	1.11	0.10	41	1957	52	1946	0.15
14.0–16.0	15.0	12.07	86.87	3.04	0.61	−0.49	55	1943	72	1926	0.15
16.0–22.0	19.0	19.81	85.33	3.66	0.68	−0.39	90	1908	92	1906	0.37
										Mean	0.18
Itapetinga creek (point 1) (S2=Site 2)[e]											
0–5	2.5	2.09	59.58	10.44	1.31	0.27	3	2002	0	2005	0
5–10	7.5	4.74	62.49	9.33	0.76	−0.27	6	1999	6	1999	0.46
10–15	12.5	7.64	72.57	5.09	1.16	0.15	10	1995	10	1995	0.74
15–20	17.5	11.21	61.13	10.07	0.65	−0.43	14	1991	17	1988	0.50
20–25	22.5	15.08	62.19	9.76	1.37	0.31	19	1986	22	1983	0.81
25–30	27.5	18.49	61.94	9.79	0.48	−0.73	24	1981	35	1970	0.26
30–35	32.5	21.29	57.61	11.51	0.46	−0.78	27	1978	41	1964	0.44
35–40	37.5	24.20	53.41	12.60	0.51	−0.67	31	1974	49	1956	0.38
40–45	42.5	26.54	48.88	14.10	1.23	0.21	34	1971	60	1945	0.21
										Mean	0.48
Itapetinga creek (point 2) (S2=Site 2)[e]											
0–5	2.5	1.53	89.00	2.04	2.15	0.76	32	1973	0	2005	0
5–10	7.5	3.06	86.83	2.66	0.32	−1.14	64	1941	6	1999	0.25
10–15	12.5	4.53	88.17	2.49	7.77	2.05	95	1910	7	1998	1.45
15–20	17.5	6.47	82.37	5.57	0.23	−1.47	136	1869	55	1950	0.04
20–25	22.5	7.69	82.02	5.77	0.16	−1.83	161	1844	59	1946	0.35
25–30	27.5	8.97	81.29	5.83	0.52	−0.65	188	1817	62	1943	0.47
30–35	32.5	10.09	46.00	17.66	1.31	0.27	212	1793	72	1933	0.10
										Mean	0.44
Porcos stream (point 3) (S2=Site 2)[e]											
0–5	2.5	1.17	64.78	8.95	0.52	−0.65	7	1998	0	2005	0
5–10	7.5	2.75	67.32	8.17	0.30	−1.20	16	1989	9	1996	0.17
10–15	12.5	3.72	67.26	8.33	0.15	−1.90	22	1983	16	1989	0.14
15–20	17.5	5.20	69.79	7.16	0.21	−1.56	31	1974	20	1985	0.36
20–25	22.5	6.47	64.89	8.67	0.18	−1.71	38	1967	27	1978	0.18
25–30	27.5	7.64	68.01	7.93	0.70	−0.36	45	1960	35	1970	0.16
										Mean	0.20
Onofre creek (point 4) (S2=Site 2)[e]											
0–5	2.5	2.29	58.24	10.77	0.62	−0.48	3	2002	0	2005	0
5–10	7.5	4.43	50.93	13.42	1.18	0.16	6	1999	2	2003	1.20

10–15	12.5	6.57	51.20	13.60	1.84	0.61	9	1996	5	2000	0.58
15–20	17.5	8.20	52.09	13.25	1.36	0.31	11	1994	12	1993	0.24
20–25	22.5	9.63	47.77	15.28	1.20	0.18	13	1992	18	1987	0.23
25–30	27.5	11.46	47.01	14.75	1.44	0.36	15	1990	25	1980	0.28
30–35	32.5	13.30	54.52	11.88	1.08	0.08	17	1988	35	1970	0.18
35–40	37.5	15.28	60.36	10.50	0.75	−0.29	20	1985	46	1959	0.18
40–45	42.5	17.17	59.11	11.40	1.30	0.26	22	1983	56	1949	0.18
45–50	47.5	19.61	65.19	9.38	0.68	−0.38	26	1979	91	1914	0.07
										Mean	0.35
Atibaia River (point 5) (S2=Site 2)[e]											
0–5	2.5	3.06	67.75	8.43	1.54	0.43	12	1993	0	2005	0
5–10	7.5	5.45	67.30	8.25	0.56	−0.58	21	1984	15	1990	0.16
10–15	12.5	8.51	70.15	7.17	0.38	−0.97	32	1973	23	1982	0.38
15–20	17.5	11.92	71.19	7.13	0.80	−0.22	45	1960	30	1975	0.50
20–25	22.5	15.03	71.07	7.56	0.20	−1.61	57	1948	52	1953	0.14
25–30	27.5	18.08	72.82	6.60	0.07	−2.66	69	1936	62	1943	0.33
30–35	32.5	20.63	74.46	6.35	0.53	−0.63	78	1927	66	1939	0.64
										Mean	0.36
Folha Larga creek (point 6) (S2=Site 2)[e]											
0–5	2.5	2.75	74.99	5.52	6.42	1.86	6	1999	0	2005	0
5–10	7.5	5.14	64.50	9.04	4.50	1.50	11	1994	11	1994	0.21
10–15	12.5	7.64	55.29	13.20	1.33	0.28	16	1989	23	1982	0.22
15–20	17.5	10.14	62.78	9.38	0.65	−0.43	21	1984	27	1978	0.58
20–25	22.5	12.79	48.98	14.95	2.53	0.93	26	1979	30	1975	1.13
25–30	27.5	16.15	50.60	14.21	2.37	0.86	33	1972	41	1964	0.30
30–35	32.5	18.49	56.07	12.13	1.05	0.05	38	1967	57	1948	0.15
35–40	37.5	21.04	58.72	11.33	1.89	0.64	43	1962	68	1937	0.24
40–45	42.5	23.89	51.61	14.34	0.74	−0.30	49	1956	108	1897	0.07
										Mean	0.36
Folha Larga creek (point 7) (S2=Site 2)[e]											
0–5	2.5	3.72	82.81	4.66	0.83	−0.19	7	1998	0	2005	0
5–10	7.5	6.32	88.97	2.81	0.52	−0.65	12	1993	14	1991	0.19
10–15	12.5	9.37	87.49	2.95	0.57	−0.56	18	1987	27	1978	0.23
15–20	17.5	12.43	78.46	5.28	0.45	−0.80	24	1981	53	1952	0.12
										Mean	0.18
Caetetuba stream (point 8) (S2=Site 2)[e]											
5–10	7.5	3.97	69.80	4.99	1.36	0.31	10	1995	0	2005	0
10–15	12.5	7.95	58.33	11.92	1.42	0.35	20	1985	8	1997	0.53
15–20	17.5	10.54	52.49	15.07	0.91	-0.09	27	1978	18	1987	0.25
20–25	22.5	13.45	54.89	11.04	0.67	-0.40	34	1971	27	1978	0.32
25–30	27.5	18.19	53.92	14.30	1.13	0.12	46	1959	36	1969	0.54
30–35	32.5	20.48	-	-	1.02	0.02	52	1953	60	1945	0.10
										Mean	0.35
Caetetuba stream (point 9) (S2=Site 2)[e]											
0–5	2.5	2.39	87.78	3.26	0.33	−1.11	3	2002	0	2005	0
5–10	7.5	6.32	75.99	5.39	0.62	−0.48	8	1997	3	2002	1.41
10–15	12.5	11.05	67.38	9.17	0.45	−0.80	15	1990	9	1996	0.79
15–20	17.5	14.67	73.62	7.02	0.52	−0.65	19	1986	14	1991	0.70
20–25	22.5	19.66	72.79	7.03	0.58	−0.54	26	1979	21	1984	0.69
25–30	27.5	22.36	67.24	9.26	0.28	−1.27	30	1975	32	1973	0.25
30–35	32.5	25.78	69.43	8.38	0.49	−0.71	34	1971	38	1967	0.51
35–40	37.5	28.22	74.88	6.70	0.16	−1.83	37	1968	55	1950	0.14
40–45	42.5	31.23	72.63	7.69	0.55	−0.60	41	1964	64	1941	0.37
										Mean	0.61
Point RX1 (S3=Site 3)[f]											
0–3	1.5	3.38	79.19	3.07	0.86	−0.15	4	2006	0	2010	0
3–6	4.5	6.86	77.81	3.42	0.67	−0.40	9	2001	4	2006	0.83

Table 1 (*continued*)

Depth range (cm)	Mean depth (cm)	Cumulative dry surface mass, CDSM (g cm^{-2})	SiO_2 (%)	LOI (%)	Excess ^{210}Pb activity, $^{210}Pb_{xs}$ (dpm/g)	ln ($^{210}Pb_{xs}$) (dpm/g)	Deposition time[a] (years) CF:CS model	Deposition year CF:CS model	Deposition time[b] (years) CRS model	Deposition year CRS model	Sedimentation rate[c] (g cm^{-2} yr^{-1}) CRS model
6–9	7.5	9.26	78.42	3.23	1.14	0.13	12	1998	8	2002	0.65
9–12	10.5	12.78	76.90	1.69	0.59	−0.53	16	1994	15	1995	0.48
12–15	13.5	16.67	76.44	3.84	1.15	0.14	21	1989	20	1990	0.84
15–18	16.5	20.52	76.10	4.10	1.09	0.09	26	1984	31	1979	0.33
18–21	19.5	24.58	75.75	4.17	0.82	−0.20	32	1978	48	1962	0.24
21–24	22.5	28.50	74.87	4.28	0.75	−0.29	37	1973	72	1938	0.16
										Mean	0.50
Point RX3 (S3=Site 3)[f]											
0–3	1.5	1.00	75.62	6.42	1.85	0.62	14	1996	0	2010	0
3–6	4.5	1.99	89.92	1.99	0.83	−0.19	28	1982	12	1998	0.08
6–9	7.5	3.37	88.75	2.07	0.69	−0.37	47	1963	19	1991	0.20
9–12	10.5	4.68	90.28	1.64	0.32	−1.14	65	1945	26	1984	0.18
12–15	13.5	6.03	89.87	2.01	0.64	−0.45	67	1943	30	1980	0.33
15–18	16.5	7.16	84.68	3.39	0.66	−0.42	69	1941	40	1970	0.11
18–21	19.5	8.52	89.23	1.77	0.53	−0.63	71	1939	55	1955	0.09
21–24	22.5	9.53	83.46	3.39	0.56	−0.58	73	1937	77	1933	0.05
										Mean	0.15
Point RX5 (S3=Site 3)[f]											
0–3	1.5	1.01	68.46	9.61	2.05	0.72	5	2005	0	2010	0
3–6	4.5	2.10	70.19	8.90	2.50	0.92	11	1999	3	2007	0.31
6–9	7.5	3.33	69.39	8.57	2.12	0.75	17	1993	8	2002	0.25
9–12	10.5	5.30	74.57	5.68	5.63	1.73	28	1982	13	1997	0.41
12–15	13.5	7.08	69.87	6.82	3.26	1.18	37	1973	31	1979	0.10
15–18	16.5	9.05	76.46	4.34	1.27	0.24	47	1963	48	1962	0.11
18–21	19.5	10.99	82.47	3.32	1.45	0.37	57	1953	59	1951	0.18
21–24	22.5	13.03	83.26	2.30	1.71	0.54	68	1942	79	1931	0.10
										Mean	0.21
Point RX6 (S3=Site 3)[f]											
0–3	1.5	2.31	58.54	9.21	1.14	0.13	18	1992	0	2010	0
3–6	4.5	5.43	64.74	7.06	1.05	0.05	41	1969	2	2008	1.69
6–9	7.5	8.87	66.95	5.52	0.85	−0.16	67	1943	4	2006	1.91
9–12	10.5	12.22	61.54	8.59	1.18	0.16	93	1917	5	2005	2.18
12–15	13.5	14.16	61.14	10.50	12.01	2.48	108	1902	7	2003	0.86
15–18	16.5	16.70	60.36	10.45	2.03	0.71	127	1883	51	1959	0.06
18–21	19.5	19.65	64.27	8.54	0.67	−0.40	149	1861	72	1938	0.14
21–24	22.5	23.05	75.06	6.49	1.48	0.39	175	1835	84	1926	0.28
										Mean	1.02
Point AMZ1 (S4=Site 4)[g]											
0–10	5	11.30	84.82	1.97	0.90	−0.10	16	1990	0	2006	0
10–20	15	25.13	84.44	1.88	0.43	−0.84	34	1972	8	1998	1.72
20–30	25	38.41	82.68	2.24	0.09	−2.41	53	1953	13	1993	2.79
30–40	35	51.61	81.98	2.62	0.23	−1.47	71	1935	14	1992	12.20
40–50	45	65.52	82.95	2.16	0.95	−0.05	84	1922	17	1989	4.81
50–60	55	79.00	82.81	2.30	0.51	−0.67	96	1910	33	1973	0.84
60–70	65	92.37	82.90	2.21	0.28	−1.27	108	1898	47	1959	0.95
70–80	75	106.34	82.75	2.31	0.30	−1.20	121	1885	58	1948	1.20
80–90	85	118.41	83.25	2.07	0.24	−1.43	132	1874	78	1928	0.60
90–100	95	130.99	82.95	2.02	0.11	−2.21	143	1863	117	1889	0.33

											Mean	2.83
Point AMZ2 (S4=Site 4)[g]												
0–10	5	10.44	78.67	2.56	1.79	0.58	23	1983	0	2006	0
10–20	15	21.15	73.40	4.43	0.52	−0.65	47	1959	10	1996	1.04
20–30	25	32.10	75.15	4.00	0.46	−0.78	72	1934	14	1992	2.97
30–40	35	43.11	75.64	3.76	0.15	−1.90	97	1909	18	1988	2.95
40–50	45	56.75	80.43	2.30	1.02	0.02	104	1902	19	1987	10.68
50–60	55	69.17	77.71	3.14	0.52	−0.65	110	1896	30	1976	1.17
60–70	65	81.22	75.39	4.15	0.68	−0.38	116	1890	37	1969	1.68
70–80	75	94.43	79.64	2.75	0.57	−0.56	123	1883	49	1957	1.04
80–90	85	107.62	80.45	2.59	0.36	−1.02	130	1876	66	1940	0.78
90–100	95	121.27	80.59	2.37	0.48	−0.73	137	1869	84	1922	0.76
										Mean	2.56
Point AMZ3 (S4=Site 4)[g]												
0–10	5	15.15	86.33	1.31	0.70	−0.36	9	1997	0	2006	0
10–20	15	29.88	83.76	1.69	0.65	−0.43	17	1989	4	2002	3.57
20–30	25	44.23	83.63	1.88	0.45	−0.80	25	1981	8	1998	3.30
30–40	35	58.46	82.94	2.09	0.34	−1.08	34	1972	12	1994	4.21
40–50	45	73.08	84.11	1.75	0.57	−0.56	40	1966	15	1991	5.22
50–60	55	85.48	77.08	3.61	0.81	−0.21	45	1961	20	1986	2.31
60–70	65	99.81	84.07	1.91	0.87	−0.14	51	1955	30	1976	1.50
70–80	75	113.55	83.98	1.90	0.45	−0.80	56	1950	44	1962	0.92
80–90	85	127.79	84.82	1.78	0.61	−0.49	62	1944	56	1950	1.21
90–100	95	142.75	85.44	1.64	0.40	−0.92	68	1938	86	1920	0.50
										Mean	2.52

[a] t=CDSM/f.
[b] Eq. (4) in the text.
[c] Eq. (5) in the text.
[d] Corumbataí River basin (Bonotto and Lima, 2006).
[e] Atibaia River basin (Sabaris and Bonotto, 2011).
[f] Ribeirão dos Bagres basin (Matamet and Bonotto, 2013).
[g] Amazon River mouth (Nery and Bonotto, 2011).

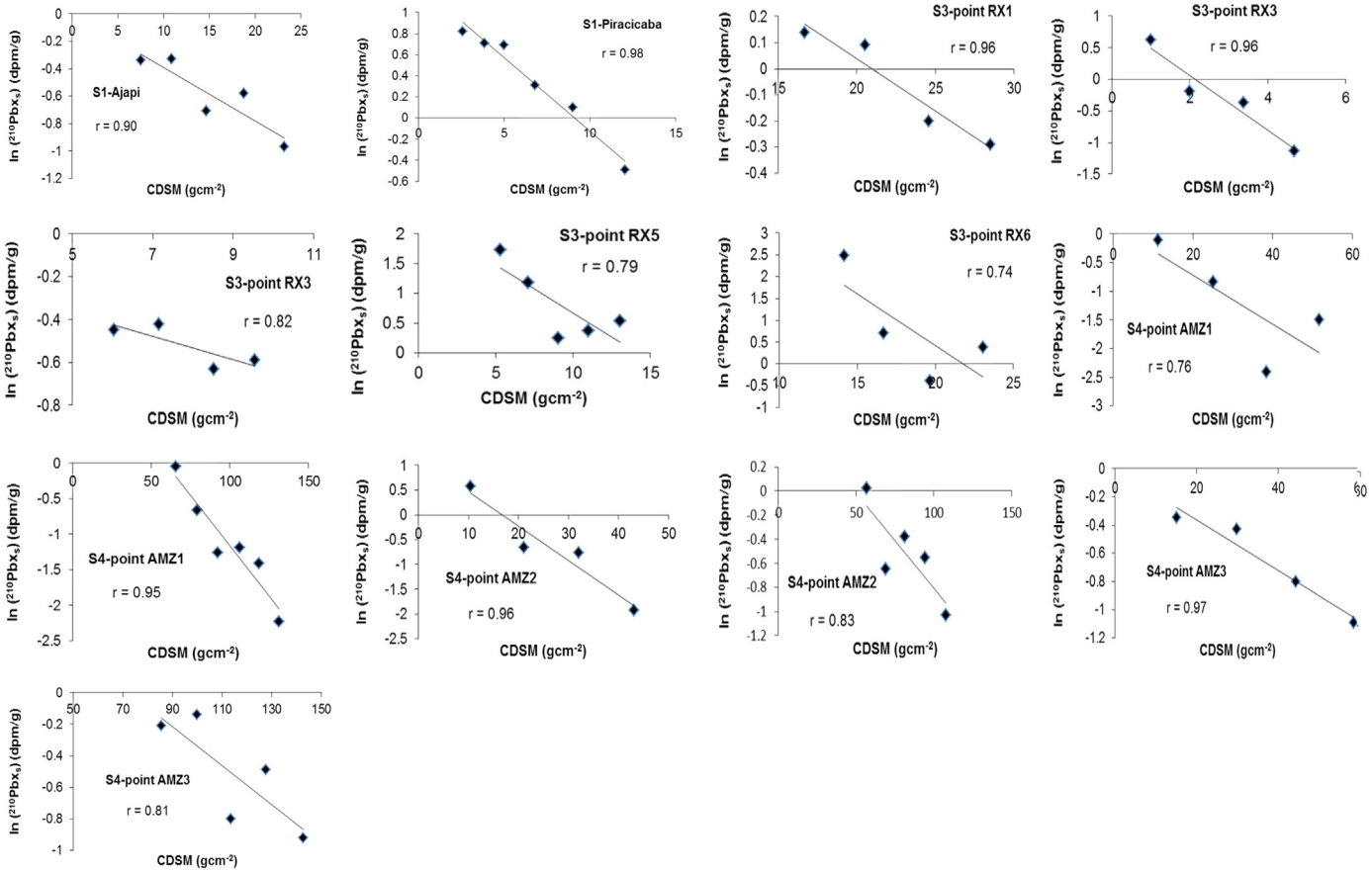

Fig. 2. Excess ^{210}Pb vs. cumulative dry surface mass (CDSM) in the sediments profiles of sites S1, S3 and S4. The data set is given in Table 1.

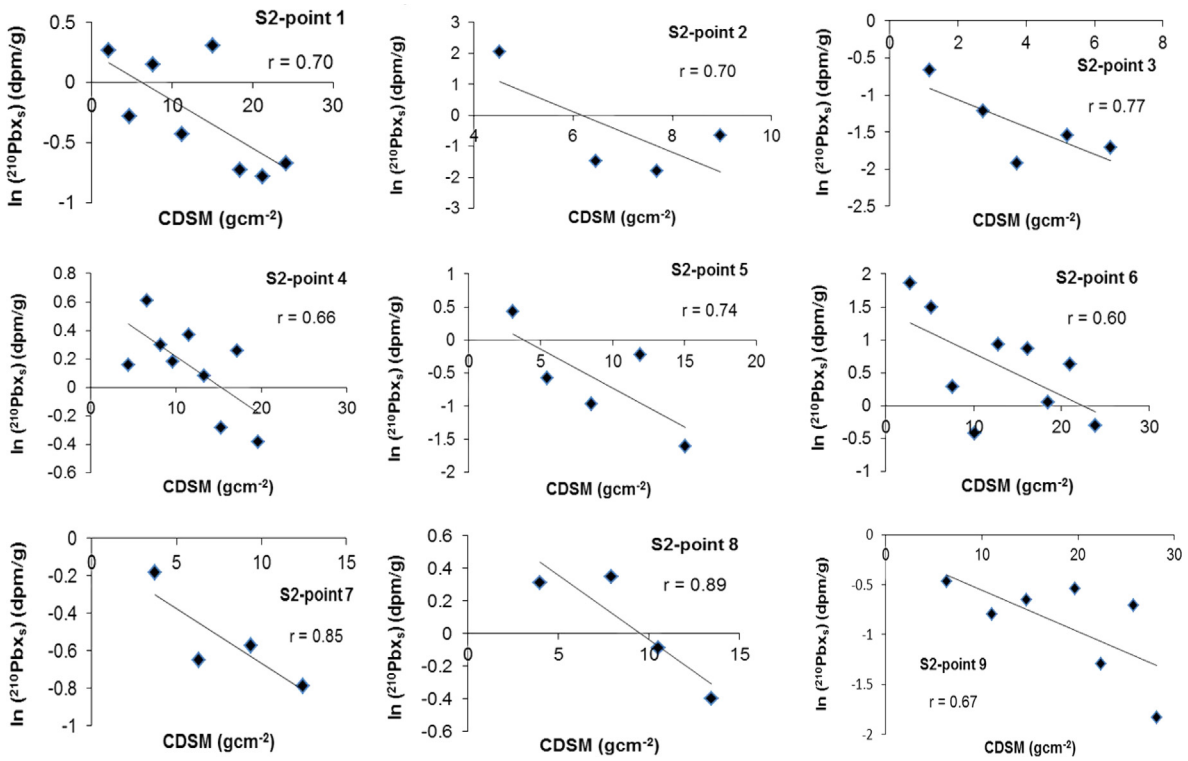

Fig. 3. Excess ^{210}Pb vs. cumulative dry surface mass (CDSM) in the sediments profiles of site S2. The data set is given in Table 1.

exhibit a congruency of predictability in the different hydrographic basins studied. However, there are some peculiar differences when checked more carefully. This can be illustrated considering the longest deposition time obtained in each sediments profile by both models as reported in Table 1. Such data are plotted in Fig. 4d, indicating non-systematic variation in each sediments core, i.e. the

Table 2
Sedimentation rates determined by the CF:CS model (Eq. (1) in the text). The slope values were found from the straight lines shown in Figs. 2 and 3.

Site	Profile	Slope	Sedimentation rate ($g\,cm^{-2}\,yr^{-1}$)	Site	Profile	Slope	Sedimentation rate ($g\,cm^{-2}\,yr^{-1}$)
S1	Ajapi	−0.039	0.80	S4	Point AMZ3	−0.018	1.74
S1	Piracicaba	−0.139	0.22	S4	Point AMZ3	−0.012	2.51
S3	Point RX1	−0.040	0.78	S2	Point 1	−0.040	0.78
S3	Point RX3	−0.434	0.07	S2	Point 2	−0.652	0.05
S3	Point RX3	−0.055	0.56	S2	Point 3	−0.183	0.17
S3	Point RX5	−0.163	0.19	S2	Point 4	−0.041	0.76
S3	Point RX6	−0.236	0.13	S2	Point 5	−0.118	0.26
S4	Point AMZ1	−0.043	0.73	S2	Point 6	−0.064	0.49
S4	Point AMZ1	−0.028	1.10	S2	Point 7	−0.059	0.53
S4	Point AMZ2	−0.070	0.44	S2	Point 8	−0.079	0.39
S4	Point AMZ2	−0.016	1.97	S2	Point 9	−0.041	0.76

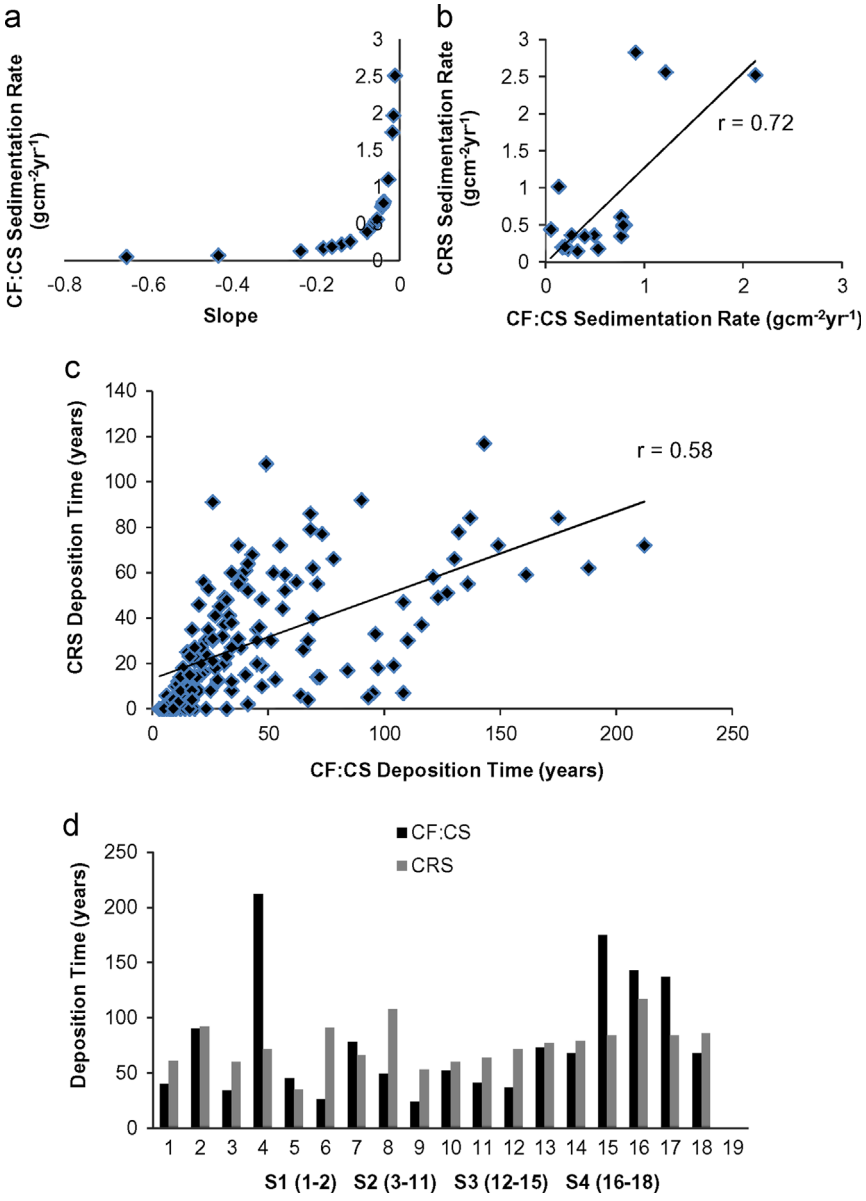

Fig. 4. The relationships between (a) sedimentation rates and best-fit straight line slopes obtained by the CF:CS model, (b) sedimentation rates obtained by the CF:CS model and mean sedimentation rates estimated by the CRS model and (c) deposition time estimated by the CF:CS and CRS models. In (d), it is plotted the longest deposition time obtained in each sediments profile by the CF:CS and CRS models.

CRS model yielded higher values in 12 cases, whereas the CF:CS model provided it in 6 situations. Furthermore, the CF:CS model predicted deposition times above 120 years in four cases: S2-point 2 (212 years), S3-point RX6 (175 years), S4-point AMZ1 (143 years) and S4-point AMZ2 (137 years). These ages are close or above of the maximum allowed by the method utilizing ^{210}Pb as a geochronometer (~150 years) and, therefore, they are not suitable for evaluating historical inputs of pollutants in the studied sites. On

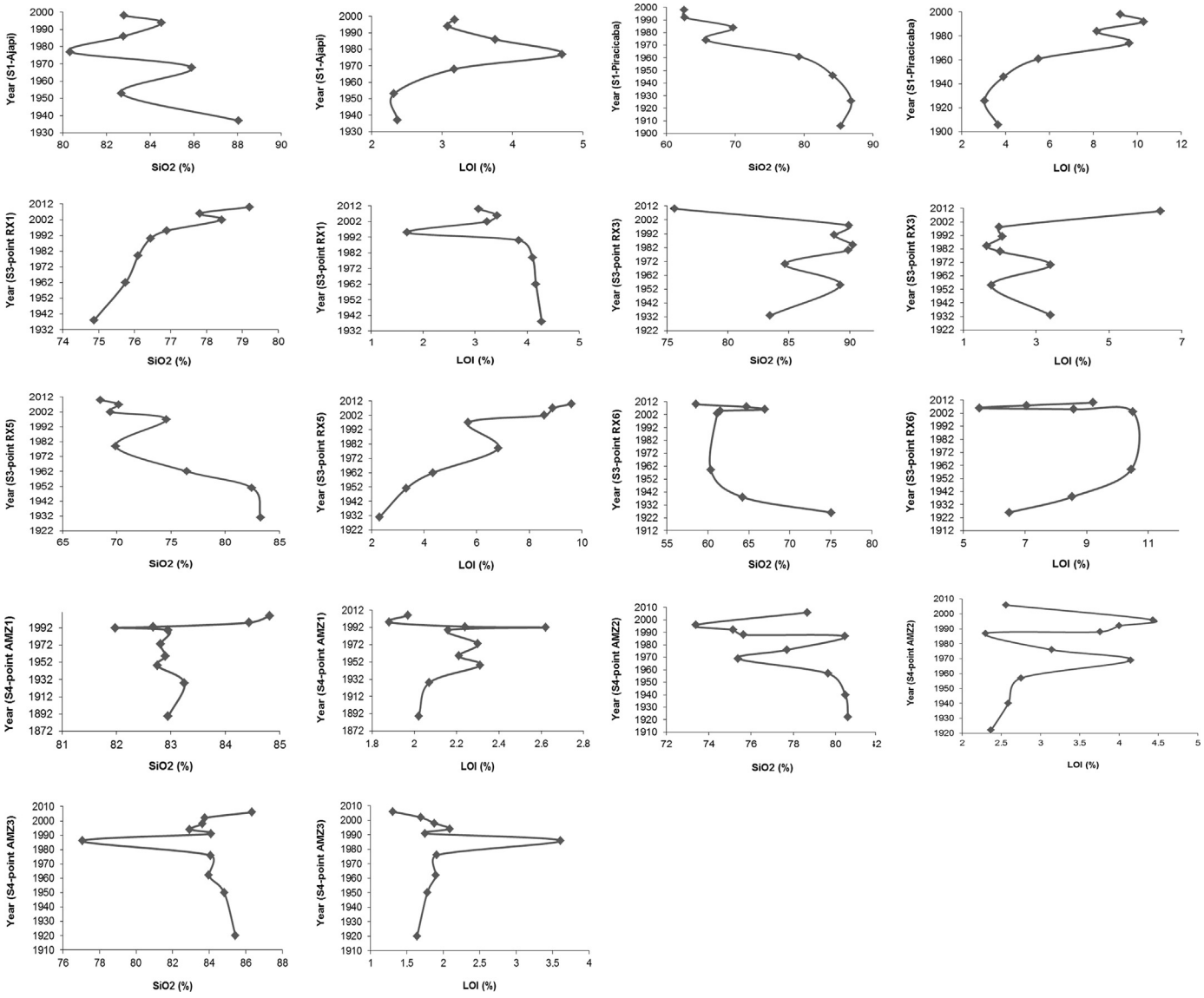

Fig. 5. The deposition year obtained by the CRS model plotted against the SiO_2 and LOI contents in the sediments profiles of sites S1, S3 and S4. The data set is given in Table 1.

other hand, the highest deposition time predicted by the CRS model corresponded to 117 years (S4-point AMZ 1) that is completely compatible with the time constraint of the ^{210}Pb-choronological method. Thus, under the chronological point of view, the performance of the CRS model was better than that of the CF:CS model in the studied sites as always provided ages within the permitted range of the ^{210}Pb-method.

Therefore, it is expected that most suitable historical trends of major compounds, trace metals or organics concentrations would be achieved from the deposition year of each sediments layer estimated by the CRS model. This has been illustrated in Figs. 5 and 6 considering the SiO_2 and LOI data given in Table 1. The sampling year and the interface water–sediments at the uppermost layer of each core have been adopted as references for the establishment of the chronology. If anthropogenic inputs are disregarded, then, the sediments composition reflects the constituents of the rocks occurring in each area studied. In all cases, they are dominated by minerals containing mainly Si and Al and minor amounts of Na, K, Ca, Fe and Mg. Silica is the major oxide of all analyzed profiles, reaching a so high value such as 90 wt% at site S3-point RX3 (depth range = 9–12 cm) (Table 1). The LOI data provides an indirect evaluation of the organic matter content in the sediments, because it expresses the organic matter + adsorbed water + water in crystal lattices and fluid inclusions + CO_2 of carbonates + SO_2 of sulfides (Faure, 1991). The LOI in the sites S1–S4 ranged from 1.3 wt% (site S4-point AMZ3; depth range = 0–10 cm) to 17.7 wt% (site S2-point 2; depth range = 30–35 cm) (Table 1).

Fig. 7 shows that the SiO_2 content decreases in accordance with the LOI (organic matter) increase in all sediments profile considered in this paper. The significance level (one-tailed probability value; 2 degrees of freedom) of the Pearson correlation coefficient obtained for the least-squares best fit was acceptable at 0.05 in all cores. The graph corresponding to the point RX1 (S3) ($r = -0.99$) was done disregarding the data of the sediments layer between 9 and 12 cm depth, due to probable analytical errors. However, even if they are included, the new Pearson correlation coefficient is $r = -0.52$ that is acceptable at 0.10 significance level.

Beyond modifying the bulk density and porosity of soils and sediments, organic matter also influences their specific surface (area per mass, often expressed in m^2/g), since 1% of organic matter in porous matrices may cause an increase of the specific

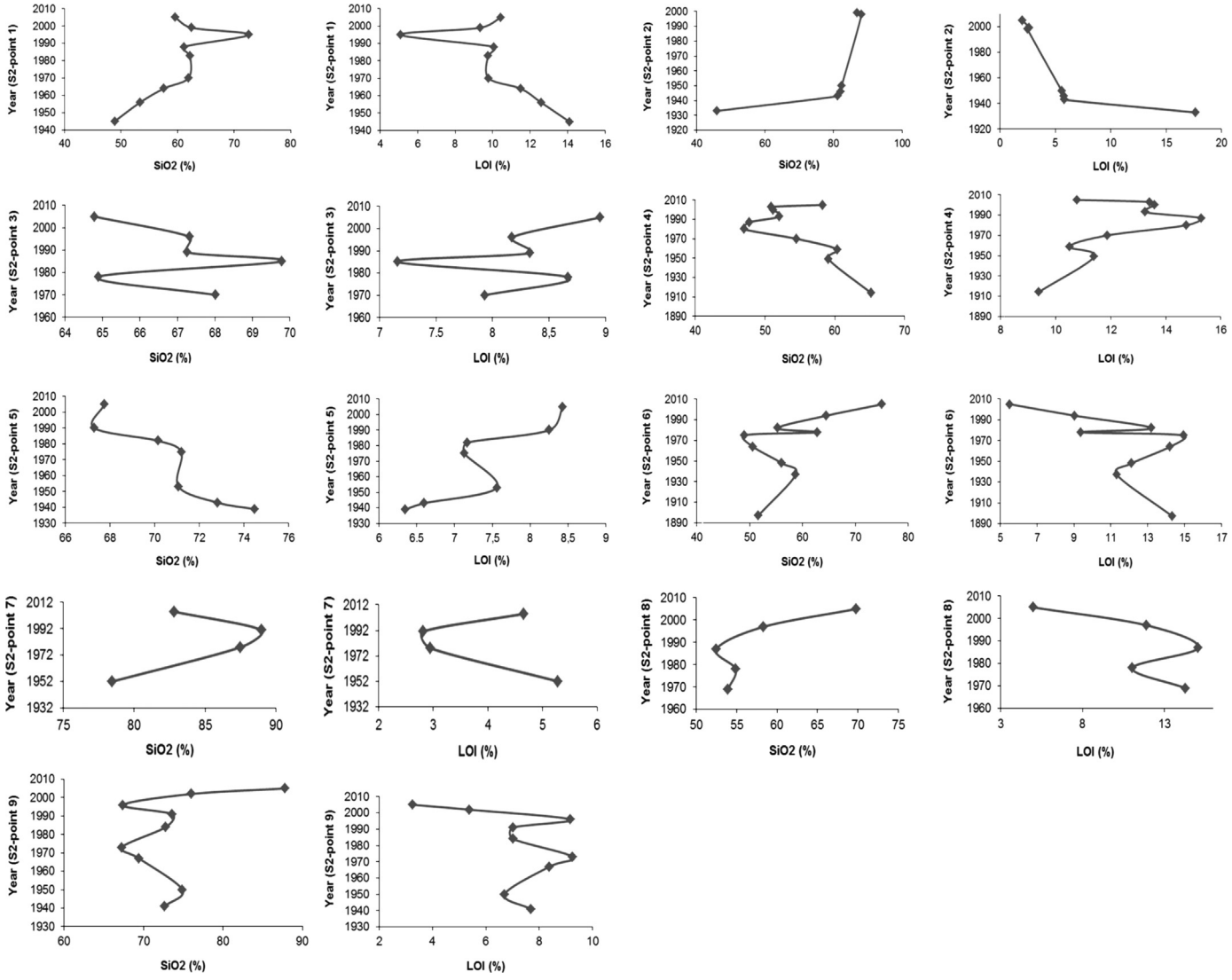

Fig. 6. The deposition year obtained by the CRS model plotted against the SiO_2 and LOI contents in the sediments profiles of site S2. The data set is given in Table 1.

surface in about 7 m^2 (Kiehl, 1977). Until 1979, most studies regarded the soil/sediment organic matter (SOM) as a high-surface-area-adsorbent in analogy with other traditional solid adsorbents (Chlou et al., 1990). However, further studies considered the aqueous-sorption and vapor-sorption behavior of soils/sediments, as well the presence of humic acids, indicating that the SOM functioned primarily as a partition medium rather than as an adsorbent in the uptake of (nonionic) organic compounds (Chlou et al., 1990).

Kaiser and Guggenberger (2008) determined the specific surface area (SSA) and the enthalpy of N_2 adsorption of separates with a density > 1.6 g cm^{-3} from 196 mineral horizons of forest soils before and after removal of organic matter with NaOCl. They concluded that mineralogy was the primary control of the relation between surface area and sorption of organic matter within some soil compartments. Thus, these findings illustrate how complexes are the relations between organic matter and surface area in sediments, claiming several methods and parameters for an in deep approach that is beyond the scope of this paper.

Anyway, there is no doubt that several parameters are significantly affected by the SOM–SSA relationship, where, in general, the cations exchange capacity, the cations adsorption, and the percentage of water retention in soils/sediments increase during the SAA rising. Therefore, the inverse relationship between silica and LOI shown in Fig. 7 suggests that the SiO_2 decrease may be accompanied by an increment in the SAA of the sediments due to the LOI enhancement.

4.3. The LOI–SiO_2 pair and historical heavy metal releases

Fallout radionuclides, including ^{137}Cs, ^{241}Am, ^{90}Sr and $^{239,240,241}Pu$ have been released into the atmosphere, deposited on the earth, and quickly adsorbed onto sediments. Their introduction into environment started in 1945 when the United States began atmospheric nuclear testing (Kathren, 1984). The nuclear weapon tests intensified in 1958–1963 and the Chernobyl atomic plant power station accident in 26th April 1986 injected a lot of artificial radionuclides in the atmosphere. Fallout can generally be divided into two types: global fallout and local (or close-in) fallout (Hong et al., 2012). Global fallout occurs when an explosion of sufficient yield occurs and the debris is injected into the stratosphere. The deposition pattern of global fallout exhibits a latitudinal dependence with maxima at mid-latitudes and minima at the poles and equator (Hong et al., 2012). This is due to the fact that large volumes of air exit the stratosphere via the tropopause discontinuity in the mid-latitudes. Since interhemispheric-stratospheric exchange of materials occurs on longer time scales than materials exchanged between the stratosphere and troposphere, most global fallout is deposited within its hemisphere of origin (Hong et al., 2012).

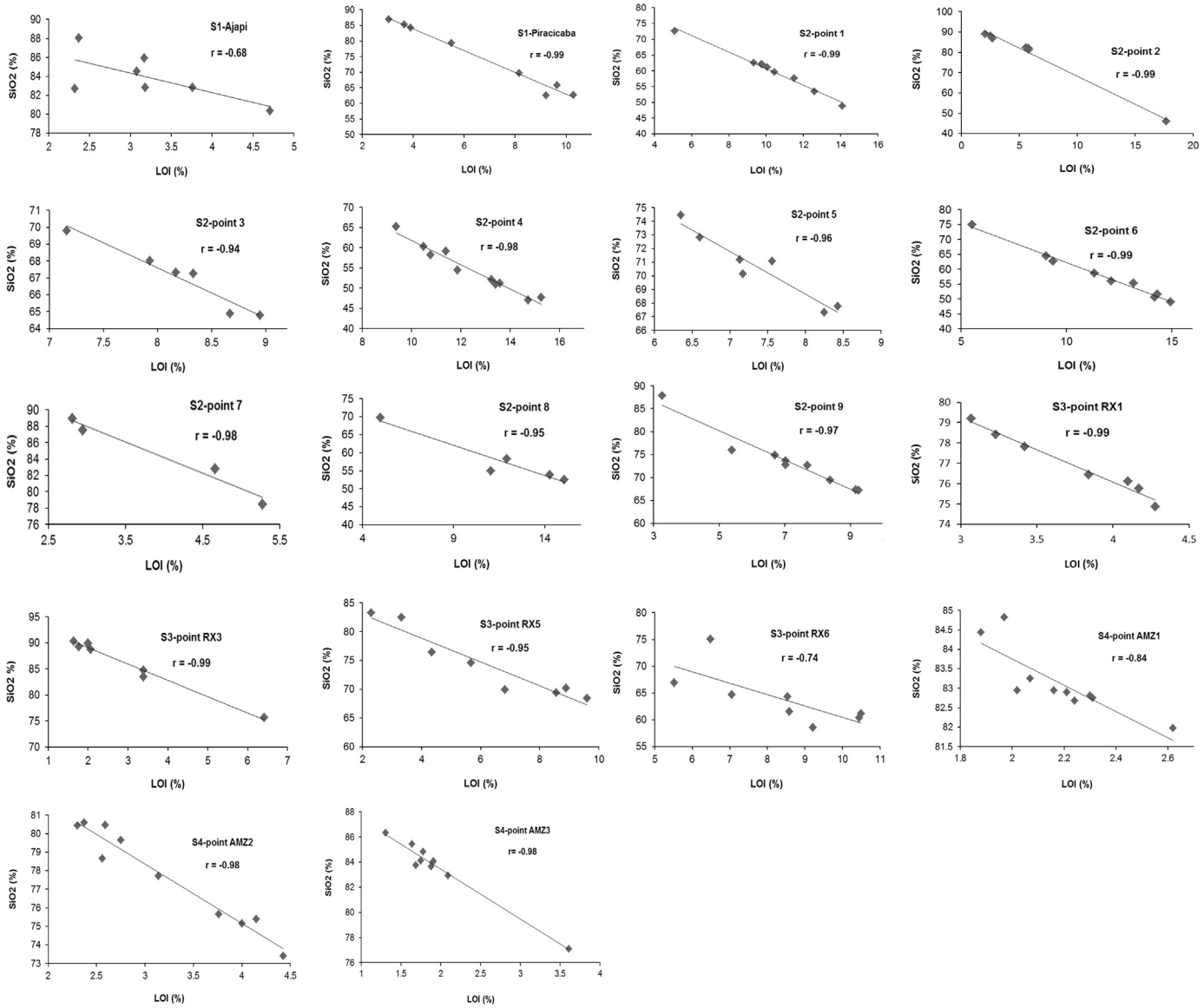

Fig. 7. The relationship between the SiO_2 and LOI contents in all sediments profiles considered in this paper. The data set is given in Table 1.

In northern hemisphere, the artificial radionuclides fallout effects in the environment have been easily identified as the atmospheric releases reached significant levels. The depositions of the principal radionuclides due to the Chernobyl accident were estimated to be 10^{17} Bq compared to 4.3×10^{17} Bq as provided from nuclear testing (Cambray et al., 1987). The estimates for ^{137}Cs reached a maximum during the mid to late 1960 of 460 PBq (4.6×10^{17} Bq), decreasing to about 170 PBq by 2010 due to its relatively short half-life (Hong et al., 2012). Of these total, approximately 76% was deposited in the northern hemisphere (between O° and 7O°N), whilst 71 PBq of ^{137}Cs should have deposited to the marine areas of the Northern Hemisphere (Hong et al., 2012).

Therefore, the depths of sediments recording activity peaks of fallout radionuclides linked to the nuclear weapon tests and the 1986 Chernobyl accident have been extensively used in northern hemisphere as an independent way of validating the results obtained by other techniques. In sediment cores, well resolved peaks of ^{137}Cs activity recording both major fallouts have been used in sediments dating, erosion prediction and to calibrate other sediments tracer methods (Kathren, 1984; Ritchie and McHenry, 1990; Abril et al., 1992; Walling and He, 1993, 1997; Abril, 2003, 2004; San Miguel et al., 2003, 2004; etc.).

Thus, since the ^{210}Pb dating is not always unambiguous, the method has been supported by dates determined from stratigraphic records of other artificial radionuclides like ^{137}Cs (see, for instance, Abril et al., 1992; Abril, 2003, 2004; San Miguel et al., 2003, 2004). This happens mainly in northern hemisphere as most global fallout has been deposited there, thus, justifying the relatively scarce radionuclides fallout data in southern hemisphere. Records of ^{137}Cs in sediments occurring in Brazil practically do not exist in part due to difficulties for finding it in detectable activities and also because of the fallout dependence with latitude that varies greatly in Brazil (from 6°N to 34°S).

These aspects give importance to the findings of the inverse relationship between SiO_2 and LOI as reported here (Fig. 7). This is because they can also be tracked in the curves of historical trends shown in Figs. 5 and 6, where high LOI values are accompanied by low SiO_2 contents and vice-versa. Some examples of very clear LOI "peaks" and corresponding SiO_2 "valleys" are: S1-Ajapi (year 1977), S1-Piracicaba (year 1974), S2-point 4 (year 1987), S2-point 6 (year 1975), S2-point 8 (year 1987), S2-point 9 (years 1996 and 1973), S3-point RX3 (year 1970), S3-point RX5 (year 1979), S4-point AMZ1 (years 1992, 1973 and 1948), S4-point AMZ2 (years 1996 and 1969) and S4-point AMZ3 (year 1986). Other examples

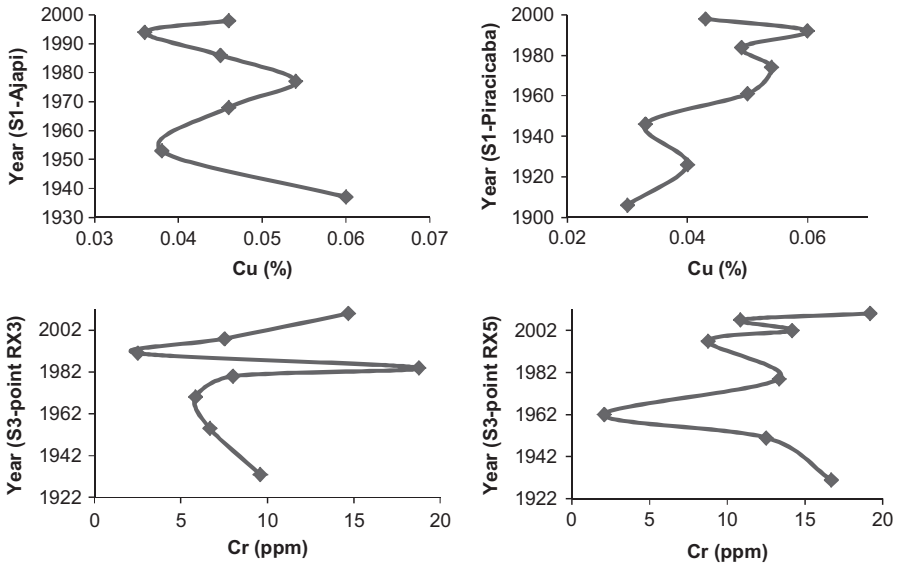

Fig. 8. The deposition year obtained by the CRS model plotted against the copper content in the sediments profile of site S1 (points Ajapi and Piracicaba) and the chromium content in S3 (monitoring points RX3 and RX5). The Cu data are reported by Bonotto and Lima (2006), whereas the Cr content is given by Matamet and Bonotto (2013).

of evident SiO_2 "peaks" and related LOI "valleys" are: S2-point 1 (year 1995), S2-point 3 (year 1985), S2-point 5 (year 1975), S2-point 7 (year 1991), S3-point RX3 (year 1984), and S3-point RX6 (year 2006).

Therefore, in the absence of an independent marker like ^{137}Cs in the sediments layers, mainly in cores providing from southern hemisphere, such findings suggest a possible use of SiO_2–LOI concentration fluctuations as an indicator of processes occurring in the past involving the hydrological systems. This is a helpful approach whose applicability may be also checked in areas occurring in northern hemisphere. In general, the major geogenic compounds in sediments are SiO_2, Al_2O_3, Na_2O, K_2O, CaO, MgO, Fe_2O_3, MnO, P_2O_5 and TiO_2, whilst the ^{210}Pb-method has been widely utilized for investigating environmental releases of heavy metals and fertilizers, among other constituents. In principle, the SiO_2–LOI concentration fluctuations could be used as well to identify heavy metal inputs in drainage basins as now considered.

Fig. 8 illustrates the curves of historical trends for Cu in S1 (Ajapi and Piracicaba) and Cr in S3 (points RX3 and RX5). Copper and chromium peaks occurring in years 1974 (S1-Piracicaba), 1977 (S1-Ajapi) and 1979 (S3-point RX5) coincide with the LOI "peaks" (and corresponding SiO_2 "valleys") at S1-Ajapi (year 1977), S1-Piracicaba (year 1974) and S3-point RX5 (year 1979) (Fig. 5). Pauli (1975) pointed out the organic matter importance on the metallic ions adsorption, considering the findings of laboratory experiments with a material derived from weathered lignin. Humic complexes of UO_2^{2+}, Pb, Cu, Zn, Ni and Cd were obtained on adding different amounts of powdered materials to the humus suspension of variable concentration. The parameters investigated were the amount of humic substance utilized as sorbent, the amount of metallic ions present in the suspension as adsorbed phase and the contact time between the two materials. The results indicated that all metallic ions combined with the humic compound utilized in the experiments. This suggests that organic matter may be taking a major role on the Cu and Cr adsorption in the sediments profiles S1-Ajapi, S1-Piracicaba and S3-point RX5.

On other hand, the Cr peak in year 1984 (S3-point RX3) (Fig. 8) coincides with a SiO_2 "peak" and LOI "valley" (Fig. 5), indicating possible preferential Cr-transport in the dominant sand matrix rather than in the organic matter fraction. The location of the sampling point RX3 in site S3 is closer to the Ribeirão dos Bagres seepage and upstream of the sewer treatment station of Franca city, São Paulo State, that are factors favoring the trends observed there.

5. Conclusion

Eighteen sediments profile from four riverine systems occurring in Brazil were subjected to a comparative evaluation of the Constant Flux: Constant Sedimentation (CF:CS) and Constant Rate of Supply (CRS) of unsupported/excess ^{210}Pb ($^{210}Pb_{xs}$) models. The selected sites possessed a reliable chemical composition and ^{210}Pb database, comprising the Corumbataí River basin (S1=Site 1, São Paulo State), Atibaia River basin (S2=Site 2, São Paulo State), Ribeirão dos Bagres basin (S3=Site 3, São Paulo State) and Amazon River mouth (S4=Site 4, Amapá State). Aliquots had been separated from sections of each core for determining the major oxides (by X-ray fluorescence) and radionuclides. Alpha spectrometry had been used to determine the ^{210}Po levels (=total ^{210}Pb), the supported ^{210}Pb had been evaluated by the eU-equivalent uranium (^{226}Ra, γ-spectrometry) or ^{238}U content (α-spectrometry) and the excess ^{210}Pb had been found by the difference between total ^{210}Pb and supported ^{210}Pb. The sediment mass fluxes by the CF:CS model were obtained by plotting the least-squares best fit of linear regressions of $\ln(^{210}Pb_{xs})$ activities against the cumulative dry surface mass data. The slopes of the best fits ranged from -0.652 (3°) to -0.012 (68°), whereas the sedimentation rates between 0.05 and 2.51 g cm^{-2} yr^{-1}, with higher slopes of the straight lines implying on greater sedimentation rates, as expected. According to the premises of the CRS model, variable sedimentation rates were found along the sediments profile, which ranged from 0 at the core surface to 12.2 g cm^{-2} yr^{-1}. Field evidences pointed out that more reliable sedimentation rates were estimated by the CRS model compared to the CF:CS model. A significant relationship was found among the deposition times calculated by the CF:CS and CRS models. However, in contrast to some CF:CS-modelled ages, the highest deposition time predicted by the CRS model corresponded to 117 years that is completely compatible with the timing constraint of the ^{210}Pb-choronological method. Silica was the major oxide of all analyzed profiles (reached up to 90 wt% at site S3), whereas the LOI content range was 1.3–17.7 wt%. The SiO_2 content decreased in accordance with the LOI increase in all cores analyzed and such inverse relationship

was also identified in the SiO_2–LOI curves of historical trends, where very clear LOI concentration "peaks" were accompanied by SiO_2 concentration "valleys" and vice-versa. In addition, it was verified as well that some SiO_2–LOI concentration fluctuations coincided with copper and chromium inputs occurring in the drainage systems of sites S1 and S3. Therefore, in the absence of an independent marker like ^{137}Cs in the sediments layers, mainly in cores providing from southern hemisphere, such findings suggest a possible use of the SiO_2–LOI concentration fluctuations as an indicator of past heavy metal releases in hydrographic basins. This is a helpful approach whose applicability may be also checked in other areas occurring in northern hemisphere.

Acknowledgments

Fundación Carolina, Madrid, Spain, is gratefully acknowledged for providing a mobility scholarship to support the sabbatical stay of D.M.B. in Universidad de Sevilla, Seville, Spain, during January and February 2014.

References

Abril, J.M., 2003. Difficulties in interpreting fast mixing in the radiometric dating of sediments using ^{210}Pb and ^{137}Cs. J. Paleolimnol. 30, 407–414.
Abril, J.M., 2004. Constraints on the use of 137Cs as a time-marker to support CRS and SIT chronologies. Environ. Pollut. 129, 31–37.
Abril, J.M., Garcia-Leon, M., García-Tenorio, R., Sanchez, C.I., El-Daoushy, F., 1992. Dating of marine sediments by an incomplete mixing model. J. Environ. Radioact. 15, 135–151.
Appleby, P.G., Oldfield, F., 1978. The calculation of ^{210}Pb dates assuming a constant rate of supply of unsupported 210Pb to the sediment. Catena 5, 1–8.
Appleby, P.G., Oldfield, F., 1992. Application of lead-210 to sedimentation studies. In: Ivanovich, M., Harmon, R.S. (Eds.), Uranium Series Disequilibrium: Applications to Environmental Problems, 2nd ed. Clarendon Press, Oxford, pp. 731–778.
Baskaran, M., Naidu, A.S., 1995. ^{210}Pb-derived chronology and the fluxes of ^{210}Pb and ^{137}Cs isotopes into continental shelf sediments, East Chukchi Sea, Alaskan Artic. Geochim. Cosmochim. Acta 59 (21), 4435–4448.
Baskaran, M., Asbill, S., Santschi, P., Brooks, J., Champ, M., Adkinson, D., Colmer, M. R., Makeyev, V., 1996. Pu, ^{137}Cs and excess ^{210}Pb in Russian Arctic sediments. Earth Planet. Sci. Lett. 140, 243–257.
Benninger, L.K., Lewis, D.M., Turekian, K.K., 1975. The use of natural Pb-210 as a heavy metal tracer in the river-estuarine system. In: Church, T.M. (Ed.), Marine Chemistry in the Coastal Environmental, 18. ACS Symposium Series, pp. 202–210.
Bonotto, D.M., 2010. The Poços de Caldas Hot Spot: A Big Blast for Nuclear Energy in Brazil. Nova Publishers, New York p. 228.
Bonotto, D.M., Caprioglio, L., 2002. Radon in groundwaters from Guarany aquifer, South America: environmental and exploration implications. Appl. Radiat. Isot. 57, 931–940.
Bonotto, D.M., Lima, J.L.N., 2006. ^{210}Pb-derived chronology in sediment cores evidencing the anthropogenic occupation history at Corumbataí River basin, Brazil. Environ. Geol. 50 (4), 595–611.
Cambray, R.S., Cawse, P.A., Garland, J.A., Gibson, J.A.B., Johnson, P., Lewis, G.N.J., Newton, D., Salmon, L., Wade, B.O., 1987. Observations on radioactivity from the Chernobyl accident. Nucl. Energy 26, 77–101.
Chlou, C.T., Lee, J.F., Boyd, S.A., 1990. The surface area of soil organic matter. Environ. Sci. Technol. 24 (8), 1164–1166.
Currie, L.A., 1968. Limits for qualitative detection and quantitative determination. Anal. Chem. 40, 586–593.
Eakins, J.D., Morrison, R.T., 1978. A new procedure for the determination of lead-210 in lake and marine sediments. Int. J. Appl. Radiat. Isot. 29, 531–536.
El-Daoushy, F., 1988. A summary on the lead-210 cycle in nature and related applications in Scandinavia. Environ. Int. 14, 305–319.
Evans, R.D., Rigler, F.H., 1980. Measurement of whole lake sediment accumulation and phosphorus retention using lead-210 dating. Can. J. Fish Aquat. Sci. 37, 817–823.
Faure, G., 1991. Principles and Applications of Inorganic Geochemistry. MacMillan Publishing Co., New York p. 626.
Flynn, W.W., 1968. The determination of low levels of polonium-210 in environmental materials. Anal. Chim. Acta 43, 221–227.
Godoy, J.M., Padovani, C.R., Pereira, J.C.A., Vieira, L.M., Galdino, S., 1998a. Aplicabilidade da Geocronologia de Deposição de Sedimentos com Pb-210 como Ferramenta na Avaliação do Assoreamento do Rio Taquari, Pantanal, MS. Geochim. Brasiliensis 12 (1–2), 113–121.
Godoy, J.M., Moreira, I., Wanderley, C., Mendes, L.B., Bragança, M.J., 1998b. A study of Guanabara bay sedimentation rates. J. Radioanal. Nucl. Chem. 227 (1–2), 157–160.
Goldberg, E.D., 1963. Geochronology with Pb-210 in radioactive dating. Int. At. Energy Contrib. 1510, 121–131.
Hong, G.H., Hamilton, T.F., Baskaran, M., Kenna, T.C., 2012. Applications of anthropogenic radionuclides as tracers to investigate marine environmental processes. In: Baskaran, M. (Ed.), Handbook of Environmental Isotope Geochemistry. Springer, Berlin, pp. 367–394.
Imboden, D.M., Stiller, M., 1982. The influence of radon diffusion on the ^{210}Pb distribution in sediments. J. Geophys. Res. 87 (C1), 557–565.
Jweda, J., Baskaran, M., 2011. A case study in southeast Michigan using excess ^{210}Pb- and ^{137}Cs-based sediment accumulation and mixing models. J. Great Lakes Res. 37 (3), 432–446.
Kaiser, K., Guggenberger, G., 2008. Mineral surfaces and soil organic matter. Eur. J. Soil Sci. 54 (2), 219–236.
Karali, T., Ölmez, S., Yener, G., 1996. Study of spontaneous deposition of ^{210}Po on various metals and application for activity assessment in cigarette smoke. Appl. Radiat. Isot. 4, 409–411.
Kathren, R.L., 1984. Radioactivity in the Environment: Sources, Distribution and Surveillance. Harwood Academic Publishers, New York.
Kiehl, E.J., 1977. Interpretação das propriedades dos solos. Teaching text, ESALQ, USP, Piracicaba, 237 pp.
Kotarba, A., Lokas, E., Wachniew, P., 2002. ^{210}Pb dating of young Holocene sediments in high-mountains lakes of the Tatra mountains. Geochronometria 21, 73–78.
Krishnaswami, S., Lal, D., Martin, J.M., Meybeck, M., 1971. Geochronology of lake sediments. Earth Planet. Sci. Lett. 11, 407–414.
Martín, J.E., García-Tenorio, R., San Miguel, E.G., Respaldiza, M.Á., Bolívar, J.P., Alves, L.C., da Silva, M.F., 2002. Historical impact in an estuary of some mining and industrial activities evaluated through the analysis by TTPIXE of a dated sediment core. Nucl. Instrum. Methods Phys. Res. B 189, 153–157.
Matamet, F.R.M., Bonotto, D.M., 2013. Evaluation of the chromium contamination at Ribeirão dos Bagres, Franca (SP), Brazil, by the ^{210}Pb method. Appl. Radiat. Isot. 82, 359–369.
Nery, J.R., Bonotto, D.M., 2011. ^{210}Pb and composition data of near-surface sediments and interstitial waters evidencing anthropogenic inputs in Amazon River mouth, Macapá, Brazil. J. Environ. Radioact. 102, 348–362.
Noller, J.S., 2000. Lead-210 Geochronology: Quaternary Geochronology – Methods and Applications. American Geophysical Union, Washington, DC.
Pauli, F.W., 1975. Heavy metal humates and their behavior against hydrogen sulfide. Soil Sci. 119 (1), 98–105.
Pennington, W., Tutin, T.C., Cambray, R.S., Eakins, J.D., Harkness, D.D., 1976. Radionuclide dating of recent sediments of Blelham Tarn. Freshw. Biol. 3, 363–382.
Ravichandran, M., Baskaran, M., Santschi, P.H., Bianchi, T.S., 1995. Geochronology of sediments in the Sabine-Neches estuary, Texas, U.S.A. Chem. Geol. 125, 291–306.
Ritchie, J.C., McHenry, R., 1990. Applications of radioactive fallout Cesium-137 for measuring soil erosion and sediment accumulation rates and patterns: a review. J. Environ. Qual. 19, 215–233.
Robbins, J.A., 1978. Geochemical and geophysical applications of radioactive lead isotopes. In: Nriagu, J.O. (Ed.), Biochemistry of Lead. Elsevier, Amsterdam, pp. 285–393.
Sabaris, T.P.P., Bonotto, D.M., 2011. Sedimentation rates in Atibaia River basin, São Paulo State, Brazil, using ^{210}Pb as geochronometer. Appl. Radiat. Isot. 69, 275–288.
San Miguel, E.G., Bolívar, J.P., García-Tenorio, R., 2003. Mixing, sediment accumulation and focusing using ^{210}Pb and ^{137}Cs. J. Paleolimnol. 29, 1–11.
San Miguel, E.G., Bolívar, J.P., García-Tenorio, R., 2004. Vertical distribution of Th-isotope ratios, ^{210}Pb, ^{226}Ra and ^{137}Cs in sediment cores from an estuary affected by anthropogenic releases. Sci. Total Environ. 318, 143–157.
San Miguel, E.G., Bolívar, J.P., García-Tenorio, R., Martín, J.E., 2001. 230Th/232Th activity ratios as a chronological marker complementing 210Pb dating in an estuarine system affected by industrial releases. Environ. Pollut. 112, 361–368.
Santschi, P.H., Presley, B.J., Wade, T.L., Garcia-Romero, B., Baskaran, M., 2001. Historical contamination of PAHs, PCBs, DDTs, and heavy metals in Mississippi River Delta, Galveston Bay and Tampa Bay sediment cores. Mar. Environ. Res. 52, 52–79.
Turner, L.J., Delorme, L.D., 1996. Assessment of ^{210}Pb data from Canadian lakes using the CIC and CRS models. Environ. Geol. 28 (2), 78–87.
Walling, D.E., He, Q., 1993. Use of Cs-137 as a tracer in the study of rates and patterns of floodplain sedimentation, tracers in hydrology. In: Peters, N.E., Hoehn, E., Leibundgut, Ch., Tase, N., Walling, D.E. (Eds.), Proceedings of the Yokohama Symposium, International Association of Hydrological Sciences (IAHS), vol. 215, pp. 319–328.
Walling, D.E., He, Q., 1997. Investigating spatial patterns of overbank sedimentation on river floodplains. Water, Air Soil Pollut. 99, 9–20.